ROMANIAN JOURNAL OF INFORMATION SCIENCE AND TECHNOLOGY
Volume **15**, Number 4, 2012, 355–367

Design Studies of Integrated Fabry-Perot Sensor Based on Bragg Grating Mirrors

Mihai KUSKO

National Institute for Research and Development in Microtechnologies,
126A, Erou Iancu Nicolae street, 077190, Bucharest, Romania
E-mail: mihai.kusko@imt.ro

Abstract. In this work the results of the theoretical studies of photonic integrated circuit refractive index sensor based on quasi1D Bragg grating configurations which act as a Fabry-Perot interferometers are presented. The variation of the medium refractive index is detected by monitoring the shift of the spectral maxima of the Fabry-Perot cavity. The sensor has been designed using the analytical expressions of the Fabry-Perot interferometer and the sensor response has been simulated with CAMFR software. The theoretical sensitivity and the detection limit are calculated and the influence of the fabrication errors on the sensor response is evaluated.

Key words: Sensor; waveguide; Fabry-Perot; Bragg gratings.

1. Introduction

The guided wave devices are extensively used in label-free biosensors due to their capacity to detect various analytes in solutions even at very small concentrations as a consequence of the interaction of the immobilized molecules at the waveguide interface with the evanescent wave. There are various types of the biosensors based on photonic integrated circuits as Mach-Zehnder interferometers, micro-ring resonators, Young interferometers and fibers based biosensors like Fiber Bragg Gratings and Fiber Long Gratings [1]. A relatively new type of sensor is based on periodic structures implemented both in fibers [2], [3] and photonic integrated circuits (photonic crystals). There are two-dimensional photonic crystals biosensors [4] and sensors based on one-dimensional photonic crystals [5], [6], [7]. The latter category include planar waveguide with Bragg grating configuration imposed by surface etching [5] and grated waveguides (waveguides with periodic variation of their width) [6], [7].

In this article a photonic integrated circuit refractive index sensor based on the Fabry-Perot interferometer is studied. The use of microcavities in sensing has been considered both for fibers [3] and waveguides [7] by monitoring the spectral shift of the transmission peaks with change of the refractive index of the medium. A sensor structure based on surface etched grating with a defect induced by a cantilever which measures the cavity maxima shift is presented in [8]. Fabry-Perot sensors could achieve low values of detection limits due to the sharp interference peaks. The structure presented here is based on a silicon nitride waveguide cavity formed by two Bragg gratings acting as high reflectance mirrors in their bandgap regions. The Bragg gratings can be obtained by surface etching of the waveguide on a relative small depth. The change of the surrounding medium refractive index induces a change of the waveguide fundamental mode effective index and subsequently a shift of cavity transmission peaks.

The aim of this paper is to study theoretically the proposed sensor. This sensor is designed by employing both analytical expressions of the Fabry-Perot interferometer and the coupled mode theory to obtain the value of the detection limit into a desired range. The numerical simulations has been performed using the planar mode expansion method [9] implemented in the photonic software package CAMFR 1.1 [10]. A comparison between the analytical and simulations results has been done in order to assess the validity of the theoretical approach. Two gratings were considered in this study: 20 nm depth grating and 50 nm depth grating, respectively. Also, the variation of the results with the fabrication errors is simulated. The entire sensor structure is modeled with a commercial software package based on Beam Propagation Method for obtaining a lossless, single-mode propagation.

The paper is structured as follows: the first section contains a description of the general lay-out of the structure. Some BPM simulations are performed in order to obtain the single-mode operation regime. The second section comprises the analytical expressions needed for designing this kind of structure. The simulation results are presented in the third section and the conclusions are summarized in the last section.

2. Layout of the structure

For simulations silicon nitride waveguides with rectangular profiles were considered. The silicon nitride is suitable for sensing applications due to its relative high refractive index [11]. The waveguide thickness is 300 nm and the waveguide substrate is a silicon dioxide layer 1700 nm thick which acts as a buffer layer between the core and the silicon substrate. The sensor analyzed here works for a wavelength range centered on 1550 nm. Due to this reason, the BPM simulations are performed for this specific radiation wavelength. The thickness of the core waveguide and the silicon dioxide are optimized in order to provide the lossless propagation for the fundamental mode of the transverse electric (TE) polarization in the waveguide on the vertical direction. The fundamental mode of the waveguide on the vertical direction for the transverse magnetic (TM) polarization is attenuated after propagation over a few millimeters due to the radiation penetration in the high refractive index silicon

substrate. To ensure the single-mode propagation in the waveguide it is necessary to achieve single-mode condition on the lateral dimension in the chip plane. The width of the waveguide can vary along propagation path.

The sensor lay-out is represented in Figs. 1a (lateral view) and 1b (top view) respectively. The selected material for configuration of the microfluidic cell is SU8 which is transparent and it has a refractive index 1.575 at 1550 nm wavelength. The refractive index of the silicon nitride is 1.98, SiO_2 refractive index is 1.46 and silicon has its refractive index equal to 3.48. The silicon nitride waveguides and the microfluidic cell can be defined by standard photolithograpy and the grating mirrors can be configured with the electron beam writing system.

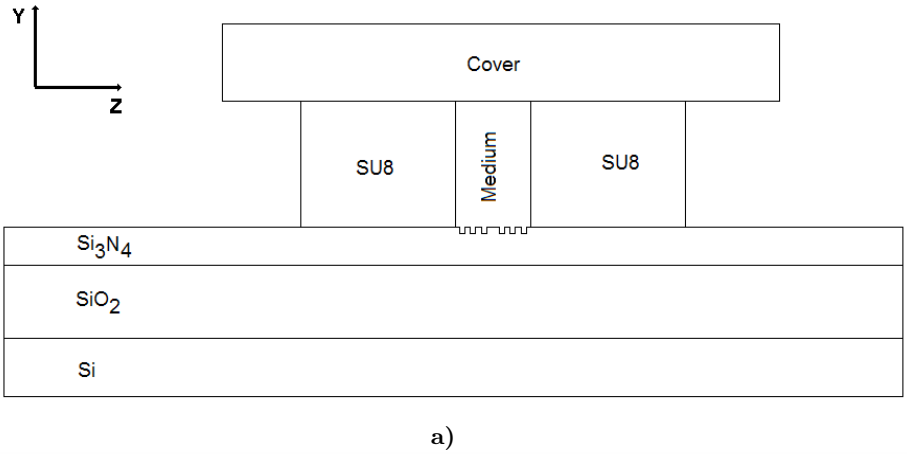

a)

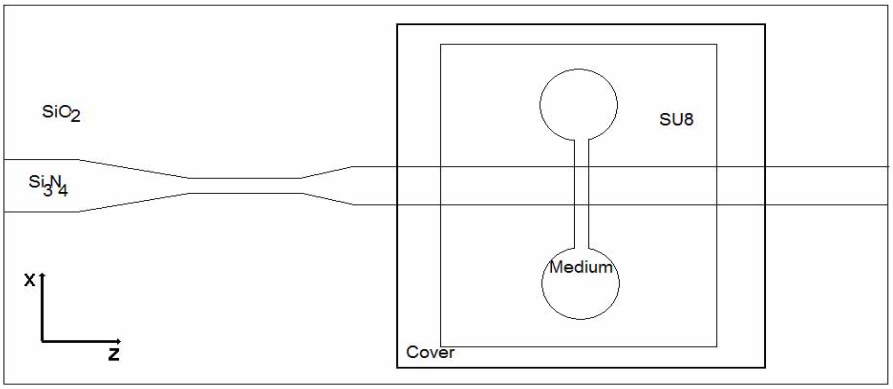

b)

Fig. 1. Schematic diagram of the sensor: a) lateral view; b) top view.

The results of radiation propagation in waveguide for both TM and TE polarization are shown in Fig. 2. The BPM simulations are performed in 2D case (lateral view) using the software package OptiBPM [12]. One can notice the rapid radiation attenuation in the case of TM polarization and the conservation of the power

inside the waveguide in the case of TE polarization. The polarization selectivity of the structure is beneficial for the sensor since the problem of the polarization maintaining is eliminated. The selectivity to radiation polarization comes from the higher penetration degree of radiation in the high index silicon substrate in the case of TM polarization compared with TE polarization.

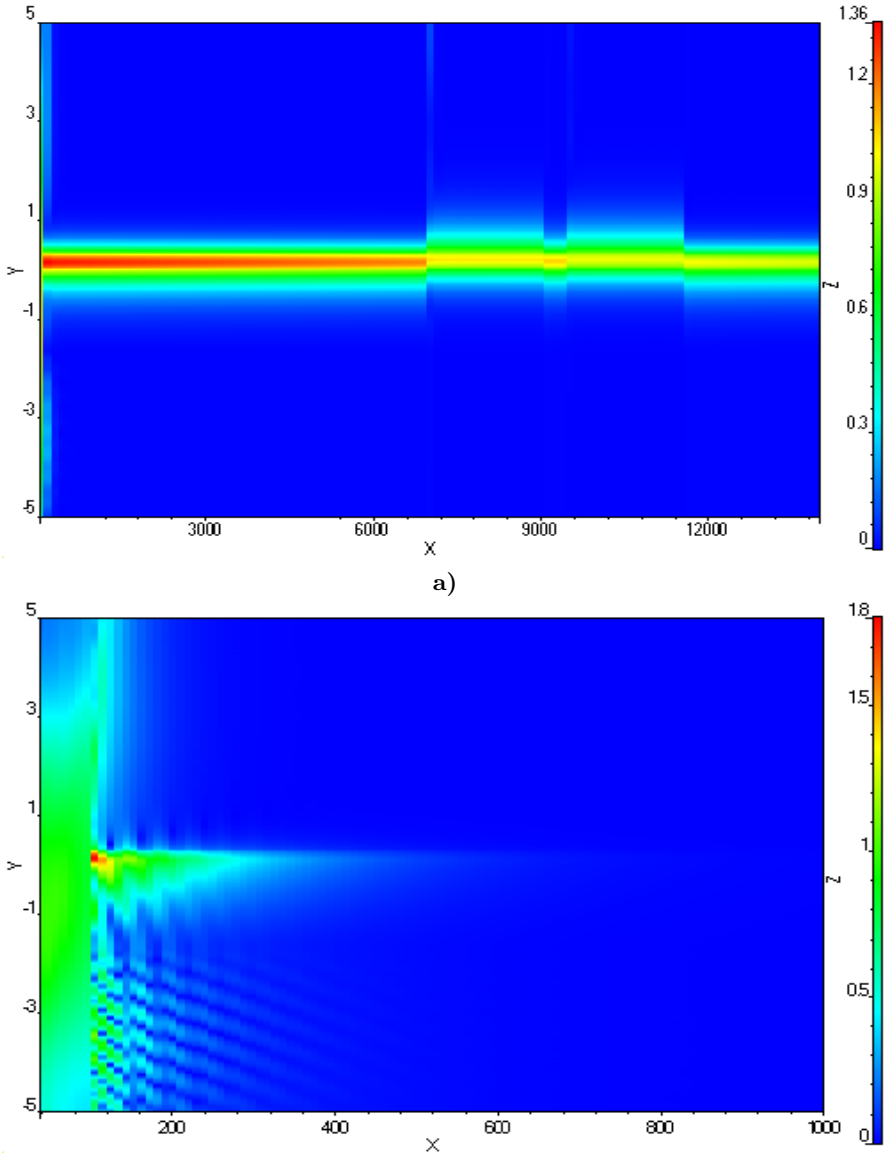

Fig. 2. Radiation propagation in the sensor structure (lateral view): a) TE polarization; b) TM polarization.

As one can see in Fig. 1b the input section is wider in order to increase the coupling efficiency and the misalignment tolerances. The waveguide width is gradually decreased via a linear tapered waveguide to 2 microns. This width is needed to ensure the single-mode propagation. The second linear tapered waveguide is considered to increase the width of the waveguide up to 4 microns in the sensing region and to maintain the propagation single-mode operation even if the waveguide become multimodal on the horizontal direction. The use of wider waveguide which retains the propagation of the fundamental mode is needed to minimize the fabrication errors which could appear if the waveguides would have the small width required for single-mode propagation over the entire length. The three dimensional simulation of radiation propagation in the structure (top view) is presented in Fig. 3.

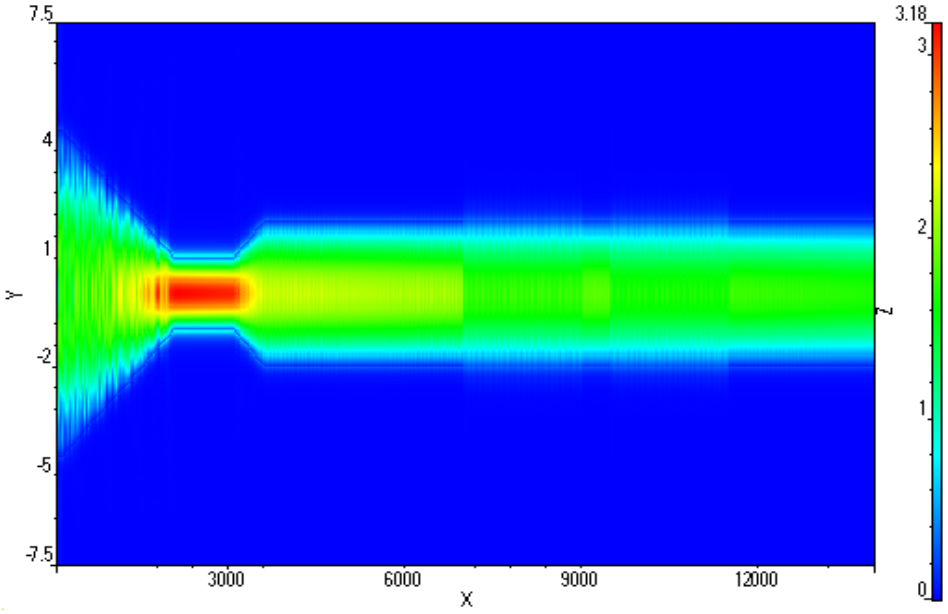

Fig. 3. BPM simulation of the radiation propagation in the sensor (top view).

3. Design

The sensor performance is defined by the detection limit (*i.e.* the minimum detectable change of the refractive index). Practically, the detection limit is associated with the noise level which depends on the measurement characteristics. Since it is difficult to estimate the noise level theoretically, the detection limit will be associated with the linewidth of the transmission peak. The value of the detection limit considered here is given by the expression:

$$DL = \frac{\delta\lambda}{15S}. \tag{1}$$

Where S represents the sensitivity expressed as the variation of the wavelength corresponding to the transmission peak over the variation of the medium refractive index. $\delta\lambda$ represents the full width at the half maximum – FWHM of the spectral line. The linewidth can be estimated from the theory of the Fabry-Perot interferometer [13] using the relation between the Free Spectral Range FSR, linewidth and the coefficient of finesse F. The minimum detectable spectral shift is the fifteenth part of the linewidth [7].

$$\frac{\delta\lambda}{FSR} = \frac{2\arcsin\left(1/\sqrt{F}\right)}{\pi}. \tag{2}$$

The coefficient of finesse dependence on the mirror reflectivity is expressed by:

$$F = \frac{4R}{(1-R)^2}. \tag{3}$$

From the above equations one can notice that the linewidth decreases with the grating reflectivity. The reflectivity of the grating mirror can be calculated with the Coupling Mode Theory approach [14]. The maximum coefficient of the reflectivity at the center of the bandgap is expressed as:

$$R = \tanh^2\left(|\kappa| L\right). \tag{4}$$

L is the length of the grating mirror and κ is the coupling coefficient. The coupling coefficient has been calculated considering the planar waveguide defined on Y-Z plane and is proportional to the grating etching depth. This approach holds for 3D configurations since the waveguide width in X-Z plane is large enough.

The free spectral range for a Fabry-Perot interferometer with Bragg grating mirror can be estimated with the standard expression:

$$FSR = \frac{\lambda^2}{2n_{eff}(L_c + 2L_{eff})}\ . \tag{5}$$

In the above expression λ is the central wavelength, n_{eff} represents the waveguide effective index, L_c stands for the length of the cavity and L_{eff} represents the effective length of the Bragg gratings. The effective length is calculated using the expression derived in [15]:

$$L_{eff} = L\frac{\sqrt{R}}{2\tanh^{-1}\sqrt{R}}\ . \tag{6}$$

Since the case of maximum grating reflectivity at the center of the bandgap is considered in this approach, the above relation is further simplified by considering the relation (4). Thus, the equation (6) is rewritten as $L_{eff} = \sqrt{R}/2\kappa$.

The sensitivity can be deduced theoretically from the following expression:

$$S = \frac{d\lambda}{dn} = \left(\frac{d\lambda}{dn_{eff}}\right)\left(\frac{dn_{eff}}{dn}\right). \tag{7}$$

The above expression can be written as:

$$S = \frac{\lambda}{n_{eff}} \left(\frac{dn_{eff}}{dn} \right). \tag{8}$$

The identity $2n_{eff}l{=}m\lambda$ and its derivative have been used to write down the relation (8). Here, l stands for the total length. The theoretical sensitivity has been deduced from the above relation and the slope of Fig. 4 which represents the variation of the waveguide effective index with the medium refractive index. The theoretical value is 127 nm/RIU (refractive index units).

Using the relations presented above for the calculation of the sensitivity and the linewidth one can design a sensor having a desired detection limit. The linewidth may be adjusted by varying both the grating reflectivity and FSR. The reflectivity of the grating increases with the etching depth and the number of periods. The FSR value is mainly inversely proportional to the length of the cavity.

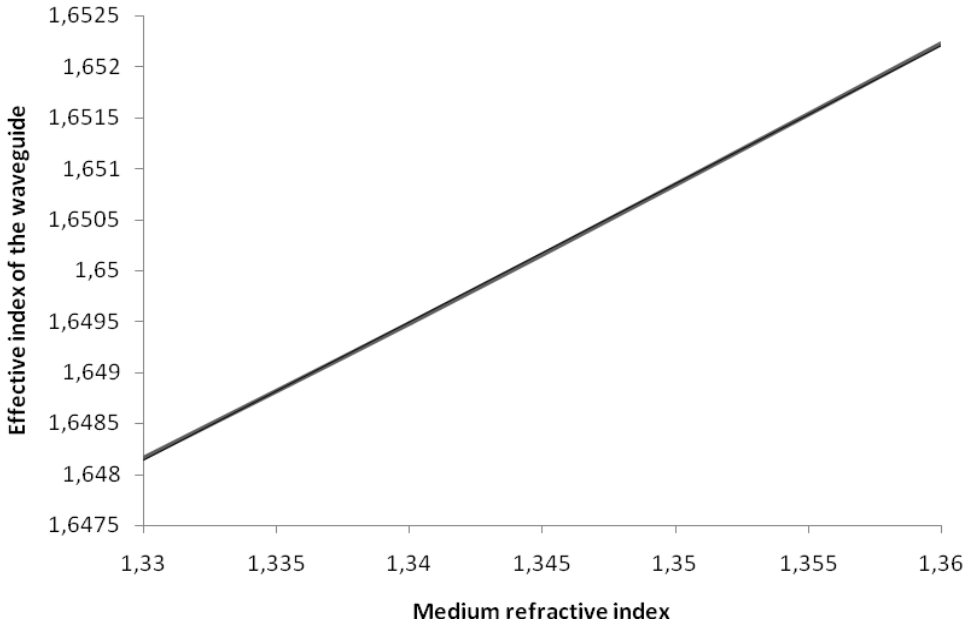

Fig. 4. Variation of the waveguide effective index with the medium refractive index.

The aim of this design study is to obtain a sensor structure with its detection limit varying in the 10^{-4} and 10^{-5} RIU range. This domain of the detection limits values have been selected only for demonstration purposes. Smaller detection limits could have been considered in this theoretical approach, but usually other experimental factors influence the detection limit at these levels. Gratings with 20 nm depth etch and 50 nm etch depth, respectively were considered in this analysis. The analytical expressions presented above were used to set the sensor parameters like number of periods and the length of the cavity in order to obtain a value for the detection limit

in the desired range. The theoretical detection limits are compared with the values obtained from simulations.

The Bragg gratings are modeled so that they render the maximum reflectivity. The length of etched and respectively the nonetched sections of the grating are set so they fulfill the condition:

$$L_{u,d} = \frac{\lambda}{4n_{eff\_d,u}} \ . \tag{9}$$

Here, n_{eff_d} and n_{eff_u} stand for the effective indexes corresponding to the etched and non etched sections, respectively. The central radiation wavelength considered here is 1550 nm. Because of the fabrication errors it is difficult to have the experimental transmission peak placed right in the center of the bandgap with a very narrow line width. As a consequence, it is necessary to design the sensor structure so that there are always at least two peaks inside the bandgap region of the spectrum. In doing this, the probability to have a transmission peak in the vicinity of the center of the bandgap is increased. The target value of the FSR is one third of the value of the bandgap.

The bandgap can be estimated theoretically using the following expression:

$$\Delta\lambda = \frac{\kappa\lambda^2}{n_{eff}\pi}. \tag{10}$$

As one can see from (10), the bandgap is increased as the coupling coefficient is larger. The theoretical value of the grating bandgap is 9 nm if the grating etch depth is 20 nm and the bandgap is 24.7 nm if the grating depth is 50 nm.

In the case of the 20 nm etching depth the length of the etched section of the Bragg grating is 237 nm and the length of the non etched section is 235 nm. The cavity is 150 μm long and each grating mirror has 200 periods. The reflectivity calculated with CMT is 0.9068. The theoretical FSR is 3.67 nm so that the linewidth is 0.12 nm. Taking in account the theoretical sensitivity one can estimate the value of the detection limit at 6.24 10^{-5} RIU.

If the grating etching depth of 50 nm is considered then the length of the etched section is 241 nm. The reflectivity for 100 periods grating mirror is 0.9773. If the cavity length is 75 μm, the value of FSR is 7.83 nm. The linewidth is 0.057 nm and the detection limit calculated theoretically is 3.03 10^{-5} RIU.

4. Simulations

Free photonic software package CAMFR 1.1 based on the mode expansion has been used to investigate the sensor response. This software is suitable to monitor the transmission of the fundamental mode through the sensor. Since this software is for 2D configurations only, the analysis has been made using the well known effective index method approach [16]. An example of how the effective index method is applied for the analysis of the gratings structures is presented in [17]. The analysis sequence of the structure is represented in Figs. 5a and 5b. At first, the effective index is

calculated on the vertical direction (Y-Z plane) for the etched and non etched section, respectively as one can see in the Fig. 5a. The values of the effective indexes are used to calculate the transmission in a new configuration in X-Z plane (see Fig. 5b). According to the effective index method theory, the results obtained for this two-dimensional configuration are similar with these obtained for the real 3D structure.

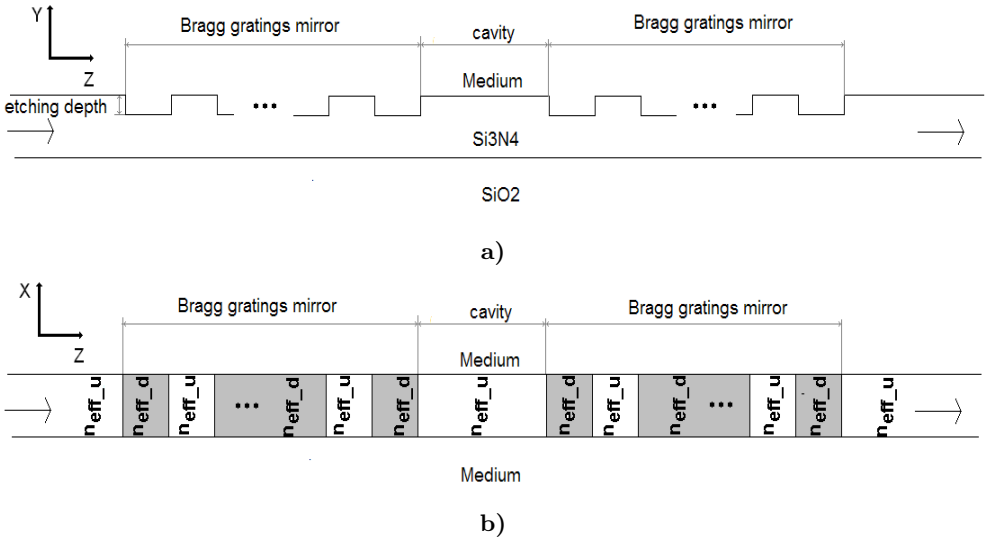

Fig. 5. Analysis sequence of the sensing structure: a) y-z structure used for the calculation of the effective indexes corresponding to the etched and non etched sections; b) x-z structure used for the calculation of the transmission.

The simulation results for the case of the gratings with 20 nm etching depth are presented in the Fig. 6. The transmission spectrum shift with the medium refractive index has been used to extract the sensitivity. The calculated value of the sensitivity is 109 nm/RIU. The simulated linewidth is 0.085 nm. The simulated detection limit is 5.2 10^{-5} RIU which is close to the value of the detection limit estimated in the previous section. The simulated FSR is about 3.1 nm. Only the narrowest peak has been considered here.

A similar analysis has been performed for the case of 50 nm etching depth. The spectral response of the Fabry-Perot cavity is shifted if the medium refractive index change from 1.33 to 1.34 as one can see in the Fig. 7.

The transmission spectrum shift has been used to extract the sensitivity and the linewidth. The calculated value of the sensitivity is 111 nm/RIU. This value is close to the theoretical value obtained for the sensitivity. The simulated linewidth is 0.04 nm. The detection limit obtained from simulation is 2.4 10^{-5} RIU, very close to the theoretical value of the detection limit estimated for this configuration. The simulated FSR is about 7.86 nm, very close to the theoretical value. As in the previous case, only the narrowest peak has been considered in this analysis.

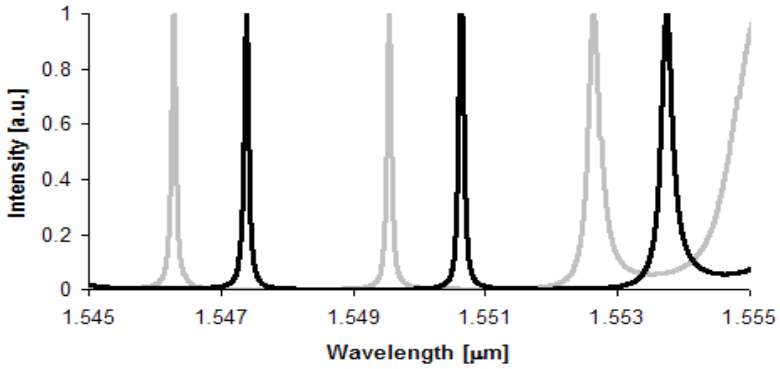

Fig. 6. Transmission spectrum for two values of the medium refractive index (grey line corresponds for n 1.33 and black line corresponds for n 1.34). The etching depth is 20 nm.

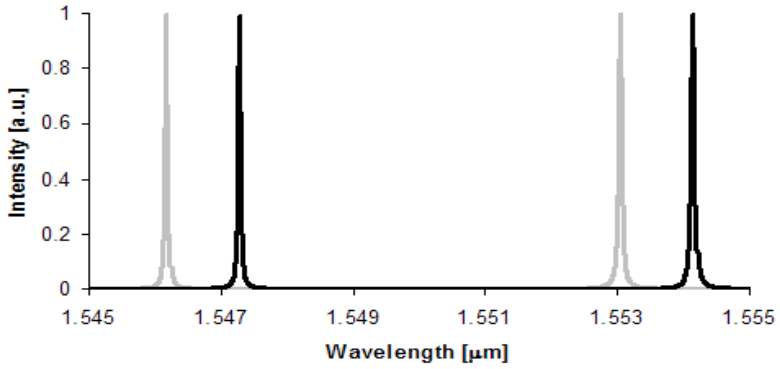

Fig. 7. Transmission spectrum for two values of the medium refractive index (grey line corresponds for n 1.33 and black line corresponds for n 1.34). The etching depth is 50 nm.

An aspect which had to be considered was the influence of the fabrication errors on the sensors performance. The fabrication errors which usually appear during the etching process may lead to an abnormal extension of the etched section of the Bragg grating with the corresponding shortening of the non etched sections. This modification of the Bragg grating parameters may lead to a decrease of the mirror reflectivity and consequently to the enlargement of the spectral transmission linewidth which in turn affects negatively the detection limit. The reflectivity of the Bragg gratings as a function of the periods number calculated with CAMFR is represented in Figs. 8a and 8b for three cases of etched section lengths both for 20 nm and 50 nm etching depth.

One can notice from the plot of the Bragg grating reflectivity versus the grating's periods number that the influence of the fabrication errors is very small for the number

of periods considered in this study. These results confirm the validity of the sensing principle. If 50 nm etching depth is considered a relative high reflectivity of about 98 percent for 100 periods is obtained which is close to the value obtained theoretically. If the etching depth is 20 nm, the reflectivity for 200 periods grating mirror is about 93 percent which is slightly higher than the reflecty value obtained from the theory.

Although there is a concordance between the simulated values of FSR and the values derived from the analytical expressions, the value of the bandgap from simulations is larger than the bandgap value derived from the relation (10). This allows the existence of more transmission peaks inside the bandgap region, thus increasing the chance to obtain a very narrow transmission peak located near the center of the bandgap.

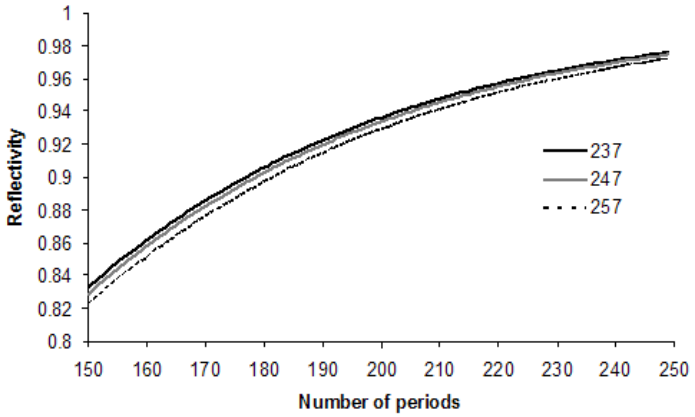

a)

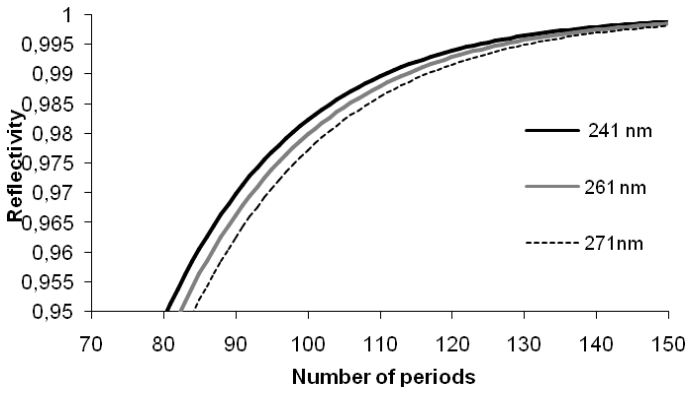

b)

Fig. 8. Reflectivity of the Bragg grating mirror function of the number of periods and the length of the etched sections: a) grating depth 20 nm; b) grating depth 50 nm.

The influence of the fabrication errors on the width of the transmission peak has been evaluated. Etching depth variation of 20 percent has been considered and also for lateral extension of the etched regions up to 20 nm has been considered. Thus, for 20 nm etching depth grating the maximal extension of the linewidth is 0.155 nm corresponding to a detection limit of 9.48 10^{-5} and for 50 nm etching depth grating the maximal extension of the linewidth is 0.145 nm corresponding to 8.7 10^{-5} detection limit.

5. Conclusions

In this work an integrated Fabry-Perot interferometer refractometric sensor with Bragg grating mirrors imposed by shallow surface etching of the silicon nitride waveguides has been studied from the theoretical point of view. The sensor is based on the spectral shift of the transmission peaks when the medium changes its refractive index. The transmission peaks are located inside the grating reflection band.

The detection limit has been estimated from the theory of the Fabry-Perot interferometer. The sensitivity, free spectral range and mirror reflectivity have been obtained using the optical waveguide theory and the coupled mode theory. Numerical simulations have been performed with CAMFR software based on the planar mode expansion method. Close results with the analytical approach have been obtained in simulations, especially for the case of Bragg gratings etched on 50 nm depth. The sensor has been optimized as a whole using the BPM simulations. A sensitive polarization, single-mode operating sensor has been designed. The numerical analysis proved that the sensor structure is robust to fabrication errors.

The results presented in this paper proves that is possible to design a sensor based on a microcavity defined by two grating mirrors with a target detection limit using an analytical approach, the data obtained theoretically being confirmed with numerical simulations performed with CAMFR software.

Acknowledgements. The research presented in this paper is supported by Sectoral Operational Programme Human Resources Development (SOP HRD), financed from the European Social Fund and by the Romanian Government under the contract number POSDRU/89/1.5/S/ 63700.

References

[1] Fan X., White I. M., Shopova S. I., Zhu H., Suter J. D., Sun Y., *Sensitive optical biosensors for unlabeled targets: A review*, Analytica Acta, **620**, pp. 8–26, 2008.

[2] Chryssis A. N., Lee S. M., Lee S. B., Saini S. S., Dagenais M., *High sensitivity evanescent field fiber Bragg grating sensor*, IEEE Photonics Technology Lett., **17**(6), pp. 1253–1255, 2005.

[3] Liang W., Huang Y., Xu Y., Lee R. K., Yariv A., *Highly sensitive fiber Bragg grating refractive index sensors*, Appl. Phys. Lett., **86**, pp. 151–122, 2005.

[4] Chow E., Grot A., Mirkarimi L. W., Sigalas M., Girolami G., *Ultracompact biochemical sensor built with two-dimensional photonic crystal microcavity*, Opt. Lett., **29**, pp. 1093–1095, 2004.

[5] Hopman W.C.L., Pottier P., Yudistra D., van Lith J., Lambeck P.V., De La Rue R.M., Driessen A., Hoekstra H.J.W.M., de Ridder R.M., *Quasi-one-dimensional photonic crystal as a compact building-block for refractometric optical sensors*, IEEE Journal of Selected Topics in Quantum Electronics, **11**(1), pp. 11–16, 2005.

[6] Kauppinen L.J., Hoekstra H.J.W.M., de Ridder R.M., *A compact refractometric sensor based on grated silicon photonic wires*, Sensors and Actuators **B 139**, pp. 194–198, 2009.

[7] Prabhathan P., Murukeshan V.M., Jing Z., Ramana P.V., *Compact SOI nanowire refractive index sensor using phase shifted Bragg grating*, Opt. Express **17**, pp. 15330–15341, 2009.

[8] Kauppinen L.J., Hoekstra H.J.W.M., Dijkstra M., de Ridder R.M., Krijnen G.J.M., *Grated waveguide optical cavity as a compact sensor for sub-nanometre cantilever deflections*, Proc. 14th European Conference on Integrated Optics (ECIO), 11–13 June 2008, Eindhoven, The Netherlands.

[9] Bienstman P., Baets R., *Optical modeling of photonic crystals and VCSELs using eigenmode expansion and perfectly matched layers*, Opt. Quantum Electron, **33**, pp. 327–341, 2001.

[10] `http://camfr.sourceforge.net`

[11] Schipper E.F., Brugman A.M., Dominguez C., Lechuga L.M., Kooyman R.P.H., Greve J., *The realization of an integrated Mach-Zehnder waveguide immunosensor in silicon technology*, Sensors and Actuators **B 40**, pp. I47–I53, 1997.

[12] `www.optiwave.com`

[13] Svelto O., *Principles of Lasers*, (New York: Plenum Press, 1989), chapter 4.

[14] Streifer W., Scifres D., Burnham R., *Coupling coefficients for distributed feedback single- and double-heterostructure diode lasers*, IEEE Journal of Quantum Electronics, **11**(11), pp. 867–873, 1975.

[15] Barmenkov Y.O., Zalvidea D., Torres-Peiró S., Cruz J.L., Andrés M.V., *Effective length of short Fabry-Perot cavity formed by uniform fiber Bragg gratings*, Opt. Express **14**, pp. 6394–6399, 2006.

[16] Nishihara H., Haruna M., Suhara T., *Optical Integrated Circuits*, (New York, McGraw-Hill, 1989), p. 31.

[17] Kauppinen L.J., *Compact integrated optical devices for optical sensor and switching applications*, PhD thesis, University of Twente, ISBN 978-90-365-3088-0, 2010.